COO-1428-273

MASTER

# Production of $K^+K^-$ and $p\bar{p}$ pairs in Four-body reactions at 13.1 GeV/c.*

J. A. Gaidos, T. A. Mulera, C. R. Ezell,

J. W. Lamsa, R. B. Willmann

Purdue University

West Lafayette, Indiana 47907

Abstract: Data in the channels $\pi^+p \rightarrow \pi^+p\,K^+K^-$ and $\pi^+p \rightarrow \pi^+p\bar{p}p$ at 13.1 GeV/c are presented; the $\Delta^{++}\,K^+K^-$ and $p\,K^+K^*(890)$ subsamples are discussed in terms of a double-Regge model. No resonance structure at $M(p\bar{p}p)$ = 3.755 GeV is observed.

*Work supported in part by the Atomic Energy Comm.

A. Introduction

We have extended an analysis of the four-constraint four-prong $\pi^+p$ interactions at 13.1 GeV/c to include $K^+K^-$ and $p\bar{p}$ pairs. The data derives from a ~ 9 event/μb equivalent exposure obtained in the SLAC 82" hydrogen bubble chamber. The r-f separated $\pi^+$ beam had a momentum spread of ~ 1.5% in the chamber; however, from the known dispersion, beam momenta were correlated with chamber coordinates and determined to ≈ .5%.

The $K^+K^-$ and $p\bar{p}$ candidates were selected from some 70,000 events which failed the $\pi^+p\pi^+\pi^-$ hypothesis [1] and for which the unbalance of measured momenta was less than 2 GeV/c. By varying the beam until momentum was conserved, the mass m in $\pi^+p \to \pi^+pm^+m^-$ was determined from energy conservation; this method was suggested and employed by Ehrlich et al. [2]. This procedure was complicated in most cases by the inability to uniquely identify $\pi^+$,p,$K^+$ components of the three positive tracks produced; for these events, permutations of identity were included. The mass spectrum of the assumed particle-antiparticle pairs thus obtained contained large contributions extending through the K and p mass values. Those combinations for which at least one permutation had $m^2 > (5\mu_\pi)^2$ ~ 13,500 events, were processed in the usual manner by the SQUAW fitting routines with $\pi^+pK^+K^-$ and $\pi^+pp\bar{p}$ four-constraint hypotheses. Each of the 1,310 events passing SQUAW was examined on the scanning table to ascertain whether observed ionizations were consistent with particle assignments of the fitted hypothesis; 560 events were acceptable. Finally a $P(\chi^2) < .1\%$ cut was imposed, reducing the sample to 468 good events. The $m^2$ distribution of those combinations which passed SQUAW is shown in Fig. 1; the solid sub-histogram corresponds to the 468 good events. The ordinate label applys strictly only to the solid area in that there are from 1 → 6 combinations possible before applying the ionization criterion. Evidently the $K\bar{K}$ and $p\bar{p}$ events are well separated in $m^2$. This selection yielded 343 $\pi^+pK^+K^-$ and 125 $\pi^+p\,p\bar{p}$ events, corresponding to cross sections of 39 ± 8μb and 14 ± 5μb respectively.

Each step in sifting the data preferentially reduced the number of event points outside of the K and p mass ranges in the $m^2$ plot, the final chi-squared cut nearly eliminating values of $m^2$ not in the desired peaks. It is apparant that selecting only on narrow $m^2$ bands about the K and p masses in the original data sample would save much labor and generate little real event loss; our choice of $m^2 > 5\mu_\pi 2$ was very conservative.

The ratios $\pi^+ p K^+K^- / \pi^+ p \pi^+ \pi^-$ and $\pi^+ p p \bar{p} / \pi^+ p \pi^+ \pi^-$ are ~ 1/30 and ~ 1/85 respectively at 13.1 GeV/c. If we define r(a) as the ratio of cross sections for $\pi^+ p \rightarrow \pi^+ p\, a\bar{a}$ production at 8 GeV/c[3] to that at 13.1 GeV/c. The data yields $r(\pi^+)$: $r(K^+)$: $r(p)$ = 1.6: 1.8: 1.1 which can be compared with $(P_{lab} = 8.0/P_{lab} = 13.1)^{-.5} = 1.3$.

B. $\pi^+ p\ K^+K^-$

A scatterplot of $M(K^-\pi^+)$ vs $M(\pi^+ p)$ is given in fig. 2, with a projection on the $M(\pi^+ p)$ axis showing a conspicuous $\Delta^{++}$ signal of ~ 99 events within the mass band $M(\Delta) = 1.24 \pm .1$ GeV. Events in the $K^*(890) - \Delta^{++}$ overlap region were divided between the $\Delta$ and $K^*$ in ratio to the population of their respective non-overlapping adjacent side bands. The projection on the $M(K^-\pi^+)$ axis is given in fig. 3(a), where the shaded portion corresponds to removal of $\Delta^{++}$ events. There are ~ 106 points in the $K^*(890)$ region defined as $M(K^*) = 0.89 \pm .1$ GeV, and in addition there is some indication of a $K^*(1420)$ signal. Removing the $K^*(890)$ band yields the shaded area in the $M(\pi^+ p)$ distribution of fig. 2. The marginal enhancement at $M(\pi^+ p) \sim 1.6$ GeV is also observed in the $\pi^+ p \pi^+ \pi^-$ data where again it is more suggestive than indicative. Within the present data, the $\Delta^{++}$ decay is described by $(1+3\cos^2\theta_J)$ where $\theta_J$ is the usual Jackson angle; the $M(\pi^+ p) \sim 1.6$ GeV region is flat in $\cos\theta_J$, and beyond $M(\pi^+ p) \sim 1.7$ GeV, the events are almost wholly within $\cos\theta_J > .8$.

The $M(K^+K^-)$ spectrum is given in fig. 3-b where the hatched area indicates removal of $K^*$ (890) events and the double hatched portion shows the $M(K^+K^-)$ distribution produced with the Δ. There is, perhaps, an indication of a shoulder in the ∅ or $S^*$ band and a modest $f^o$ and/or $A_2{}^o$ signal. Selecting on the Δ does not sharpen the $f^o/A_2$ signal, a result evidently different from the 8 GeV data.[3] A preliminary sample of ~ 50 events in the $\pi^+ p K^o \bar{K}^o$ channel also shows no ∅ signal, and comparably modest $f^o/A_2{}^o$ production.[4] The $M(K^-p)$ spectrum suggests no clear resonance formation.

A low mass enhancement is evident in the $M(K^+K^-\pi^+)$ distribution in fig. 4. The hatched area remains after removed of $\Delta^{++}$ events and the double-hatched part is left following the further substraction of $K^*(890)$ events. A possible explanation of the $M(K^*K)$ threshold enhancement will be given in the following section.

C. $K^*Kp$

The $K^*Kp$ subsample of the data is characterized by low four-momentum transfers $t(\pi K^*)$, $t(\pi K)$ and $t(pp)$ and consequently a tendancy towards low values of $M(K^*K)$; these features are reminiscent of the $(\rho\pi)$ behaviour through the $A_1$ enhancement region and suggest that a similar interpretation in terms of a double-exchange peripheral amplitude may be appropriate [1]. By requiring $-t(\pi K^*)$ and $-t(\pi K) < 2.0\ (GeV/c)^2$ and $-t(pp) < 0.5\ (GeV/c)^2$ a peripheral set of 60 events is obtained with the t-distributions shown in fig. 5; also pictured is the double-Regge diagram assumed. The amplitude was taken as

$$A(K^*, Pom.) = R(K^*) \cdot (S_{KK^*}/S_o)^{\alpha_{K^*}} e^{4 t_{pp}} (S_{K^*p}/S_o)^{\alpha_{Pom}}$$

with the usual Reggeized $K^*$ -exchange propogator $R(K^*)^\dagger$ and a linear trojectory $\alpha_{K^*} = 1 - \alpha''(0)_{K^*} [M_{K^*}{}^2 - t]$. The values $\alpha'(0)_{K^*} = 1\ (GeV/c)^2$ and $S_o = 1\ (GeV/c)^2$ are used throughout. Pomeranchuk exchange is described by $\alpha_{Pom.} = 1$ and an exponential residue determined from elastic scattering. The predictions are normalized to the data and comparisons to the t-spectra and mass distributions are shown in fig. 5 and fig. 6 respectively. Evidently there is no necessity to include a diagram involving K-exchange ($K^*$ and K positions interchanged).

Duality arguments would suggest that the observed $M(K^*K)$ threshold enhancement corresponds to the existence of a resonance in the $KK^*$ system at a low mass value; in addition to the $A_3(1640)^{\dagger\dagger}$, there is a reported abnormal (spin-parity) state decaying into the $KK^*$ channel with a mass of 1.54 GeV, listed as the $F_1$.[5]

D. $K^+K^-\Delta^{++}$

A description of the $K^+K^-\Delta$ channel is given in terms of the double-exchange diagram shown in fig.7. There are 49 events within the kinematical region defined by $-t(\pi K^+) < 1.0\ (GeV/c)^2$ and $-t(p\Delta) < 0.5\ (GeV/c)^2$. The double-Regge amplitude assumed to describe this data is taken as:

$$A(K^*\pi) = R(K^*)\ (S_{K^+K^-}/S_o)^{\alpha_{K^*}}\ .\ R(\pi)\ (S_{K^-p}/S_o)^{\alpha_\pi}$$

with $\alpha_\pi = -(\mu_\pi^2 - t(p\Delta))$ and $R(K^*)$ as in section C. The t distributions and mass spectra are given in fig. 7 and fig. 8 respectively along with curves representing the predictions of $A(K^*\pi)$. Although sparse, the data are well described by the double-exchange mechanism.

E. $\pi^+p\bar{p}p$

Both combinations of $M(\pi^+p)$ are shown in fig. 9-a where $\Delta$ production is clearly evident, with approximately 30% of the reaction involving a $\Delta$. The curve in fig. 9-a is the prediction of phase space. There is no suggestion of a resonant state at 3.755 GeV in the $M(p\bar{p}p)$ distribution shown in fig. 9-b; the only deviation from phase space is the high mass peaking which reflects $\Delta$ formation in $M(\pi^+p)$.[3] The $M(\bar{p}p)$ spectrum is given in fig. 10; the two small enhancements in the low mass range may correspond to production of $N\bar{N}(2190)$ and $\rho(2290)$ respectively.[6]

F. Conclusion

The reaction $\pi^+p \rightarrow \pi^+pK^+K^-$ occurs with a frequency of 1/30 th of that of the $\pi^+p\pi^+\pi^-$ channel; whereas the latter is dominated by $\rho$, $f^o$ and $\Delta^{++}$ production, the former consists mostly of the $K^*(890)$ and $\Delta^{++}$ states, each of which constitutes ~ 30% of the reaction; there is some evidence for a $K^*(1420)$. The significant difference is the lack of two-particle final states in the $K^+K^-$ case, no evidence for a strong $\phi$ (e.g.) is observed. The data are consistent with the predictions of double-Regge exchange; $K^*$/Pomeranchuk exchanges in the $K^+K^-p$ state and $K^*/\pi$ exchanges in the $\Delta^{++}K^+K^-$ channel. The $\pi^+p \rightarrow \pi^+\bar{p}pp$ reaction is 2.8 times less frequent than the $\pi^+pK^+K^-$ state. Formation of $\Delta^{++}$ occurs in ~ 30% of these events with the remainder evidently following phase spare. At resonance at $M(\bar{p}p)$ = 3.755 GeV, reported by Ehrlich et al. [2], was not observed.

(1) J. A. Gaidos, C. R. Ezell, J. W. Lamsa, and R. B. Willmann, Phys. Rev. Vol. 2 D(1970) 1226.

(2) R. Ehrlich, R. J. Plano, and J. B. Whittaker, Phys. Rev. Letters 20 (1968) 686.

(3) M. Aderholz et al., Nucl. Phys. B14 (1969) 255.

(4) J. Tebes, private communication, to be published.

(5) M. Aguilar-Benitez et al., Nucl. Phys. B14 (1969) 195.
M. Aguilar-Benitez et al., Phys. Letters 29B (1969) 379.

(6) Reviews of Particle Properties, Phys. Letters 33B (1970).

FOOTNOTES

† $R(i) = \frac{[1 + \tau_i e^{-i\pi\alpha_i}]}{\Gamma(1 + \alpha_i) \sin(\pi\alpha_i)}$

†† The possibility that the low mass $KK^*$ enhancement is a decay made of the diffractively produced $A_3(1640)$ is under investigation.

FIGURE CAPTIONS

Fig. 1. Distribution in $m^2$ for the reaction $\pi^+ p \rightarrow \pi^+ p m^+ m^-$ at GeV/c of those event combinations for which a fit was obtained with $m = M_K$ or $K_p$. The solid area indicates the $m^2$ distribution of the final good event sample.

Fig. 2. Scatterplot of $M(K^-\pi^+)$ vs. $M(\pi^+ p)$ axis. An event with $|M(\pi^+ p)-1.236| < 0.1$ GeV was accepted as a $\Delta^{++}$; the solid area corresponds to the removal of $K^*(890)$ points.

Fig. 3. (a) Distribution in $M(K^-\pi^+)$; the hatched portion remains after $\Delta^{++}$ Subtraction.

(b) Distribution in $M(K^+K^-)$ ; removal of $K^*(890)$ events yields the hatched area and selecting on the $\Delta^{++}$ gives the cross-hatched spectrum.

Fig. 4. Distribution in $M(K^+K^-\pi^+)$; removing $\Delta^{++}$ events gives the hatched spectrum; further removal of $K^*(890)$ data yields the cross-hatched area.

Fig. 5. Four-momentum transfer distributions in the process $\pi^+ p \rightarrow pK^+K^*(890)$; the curves represent the prediction of the double-exchange diagram shown.

Fig. 6. Invariant mass distributions in the reaction $\pi^+ p \rightarrow pK^+K^*(890)$; the curves are from the double-Regge model.

Fig. 7. Four-momentum transfer distributions in the process $\pi^+ p \rightarrow \Delta^{++} K^+K^-$; the curves represent the predictions of the double-exchange diagram shown.

Fig. 8. Invariant mass distributions in the reaction $\pi^+ p \rightarrow \Delta^{++} K^+K^-$; the curves are from the double-Regge model.

Fig. 9. (a) Distribution in $M(\pi^+ p)$ of the reaction $\pi^+ p \rightarrow \pi^+ p\bar{p}p$ at 13.1 GeV/c.

(b) Distribution in $M(p\bar{p}p)$ of the reaction $\pi^+ p \rightarrow \pi^+ p\bar{p}p$ at 13.1 GeV/c.

Fig. 10. Distribution in $M(\bar{p}p)$ of the reaction $\pi^+ p \rightarrow \pi^+ p\bar{p}p$ at 13.1 GeV/c.

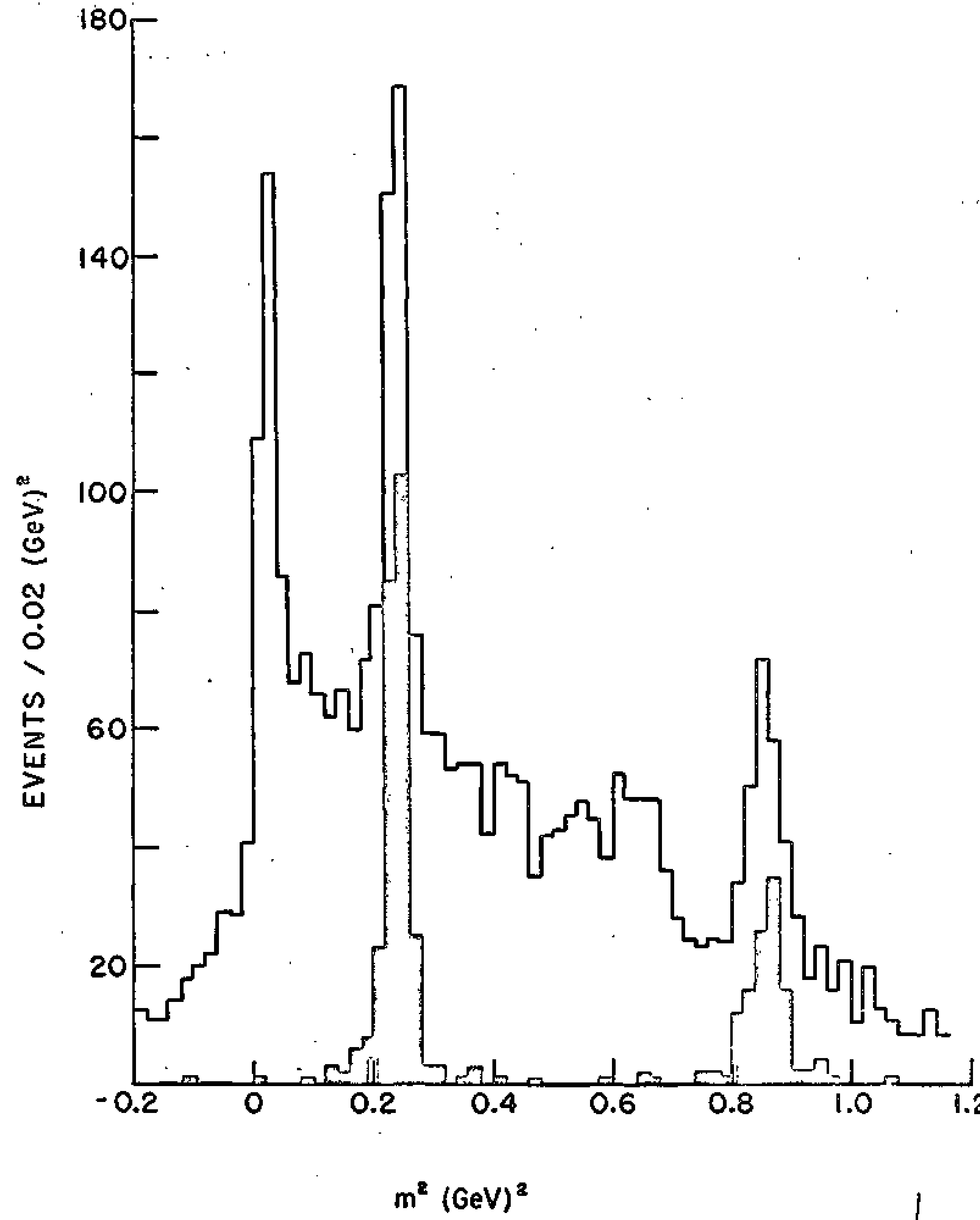
180
140
100
60
20
EVENTS / 0.02 (GeV)²
-0.2
0
0.2
0.4
0.6
0.8
1.0
1.2
m² (GeV)²

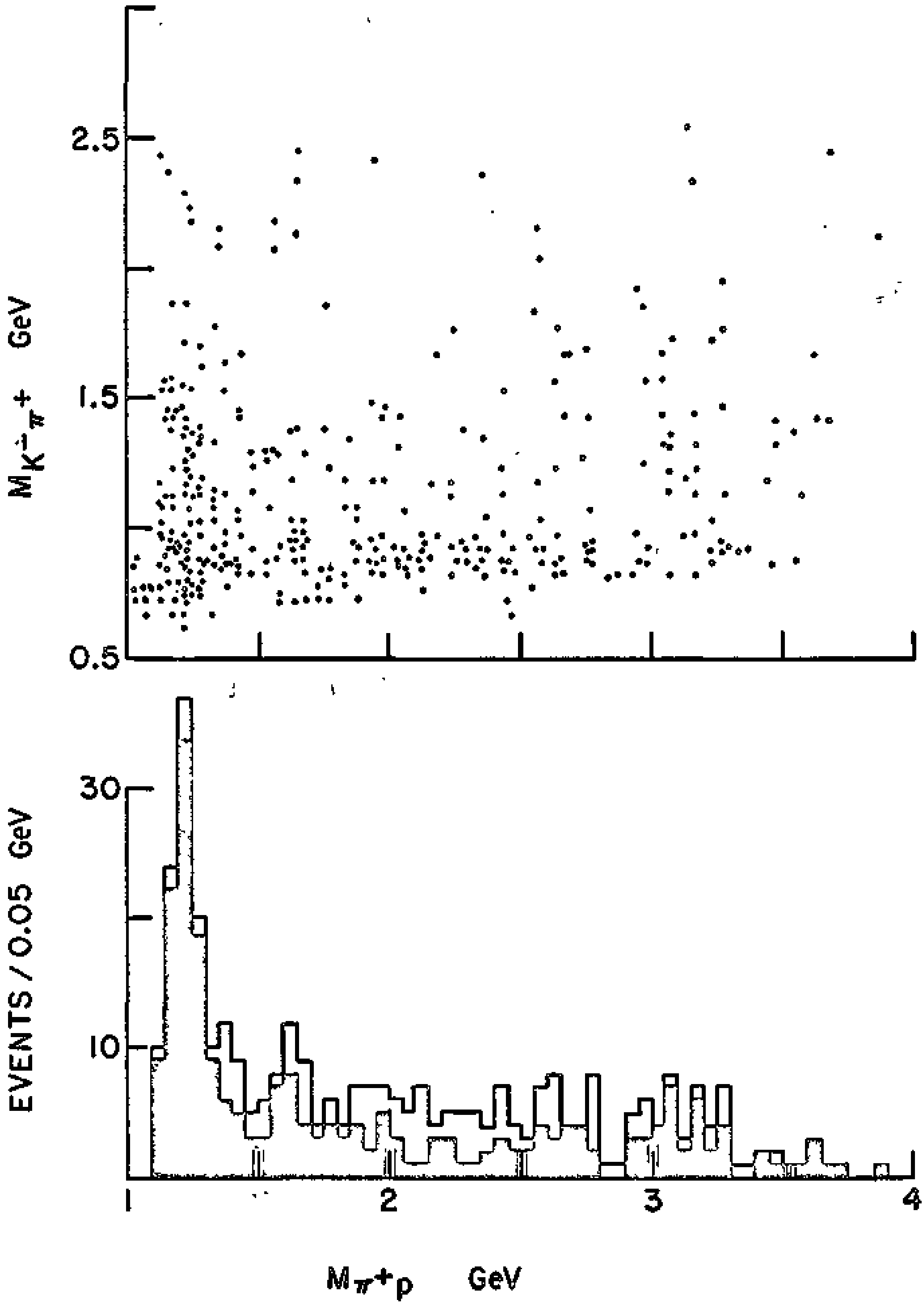

2.5
1.5
0.5
$M_{K^{\pm}\pi^+}$ GeV
30
10
EVENTS / 0.05 GeV
1
2
3
4
$M_{\pi^+p}$ GeV

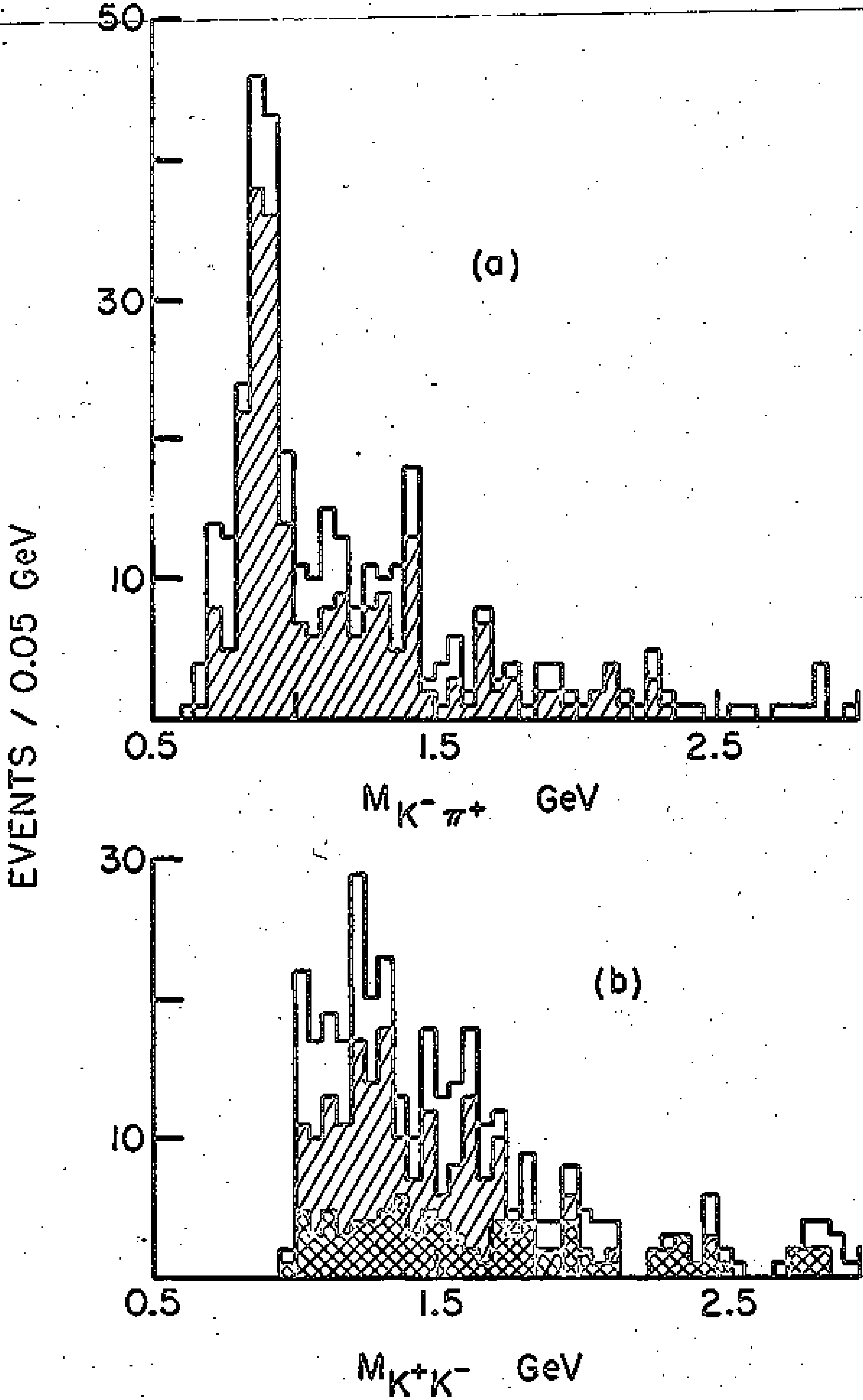

EVENTS / 0.05 GeV
50
30
10
(a)
0.5
1.5
2.5
$M_{K^-\pi^+}$ GeV
30
10
(b)
0.5
1.5
2.5
$M_{K^+K^-}$ GeV

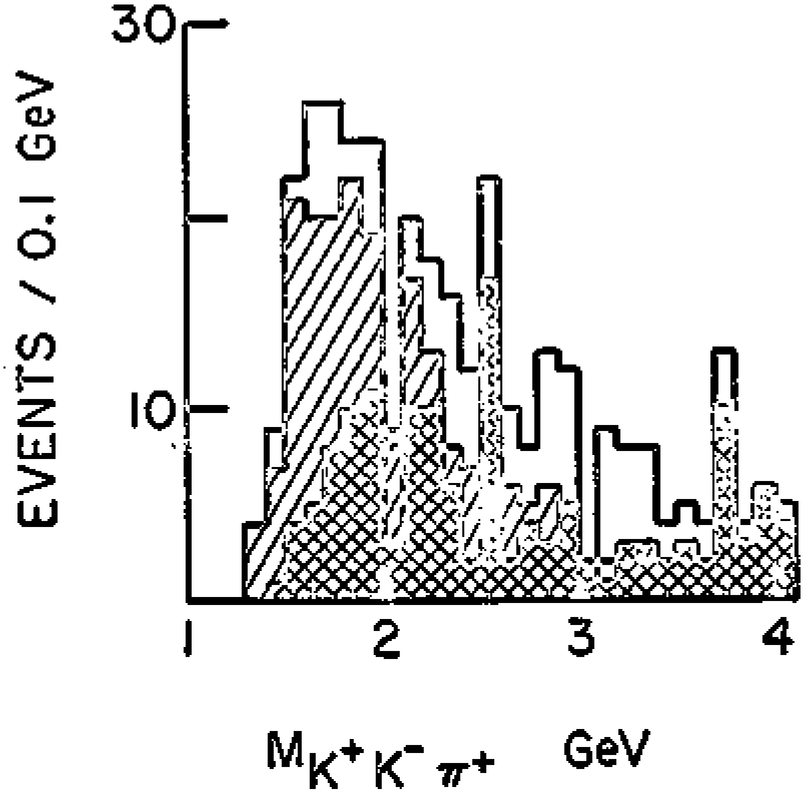

30
10
EVENTS / 0.1 GeV
1
2
3
4
$M_{K^+K^-\pi^+}$ GeV

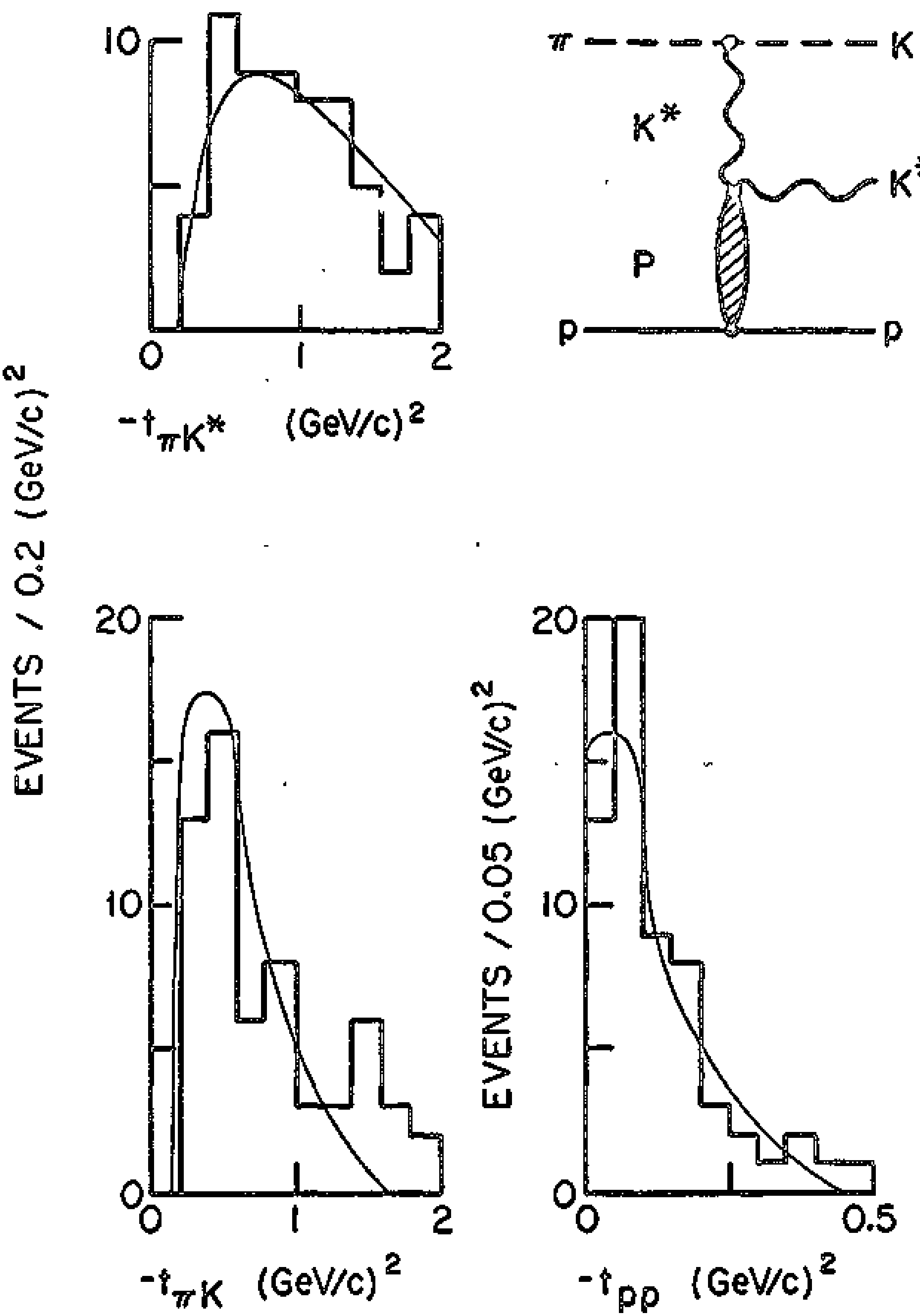
10
0
1
2
$-t_{\pi K^*}$ (GeV/c)$^2$
π
K
K*
K*
P
p
p
EVENTS / 0.2 (GeV/c)$^2$
20
10
0
0
1
2
$-t_{\pi K}$ (GeV/c)$^2$
EVENTS / 0.05 (GeV/c)$^2$
20
10
0
0
0.5
$-t_{pp}$ (GeV/c)$^2$

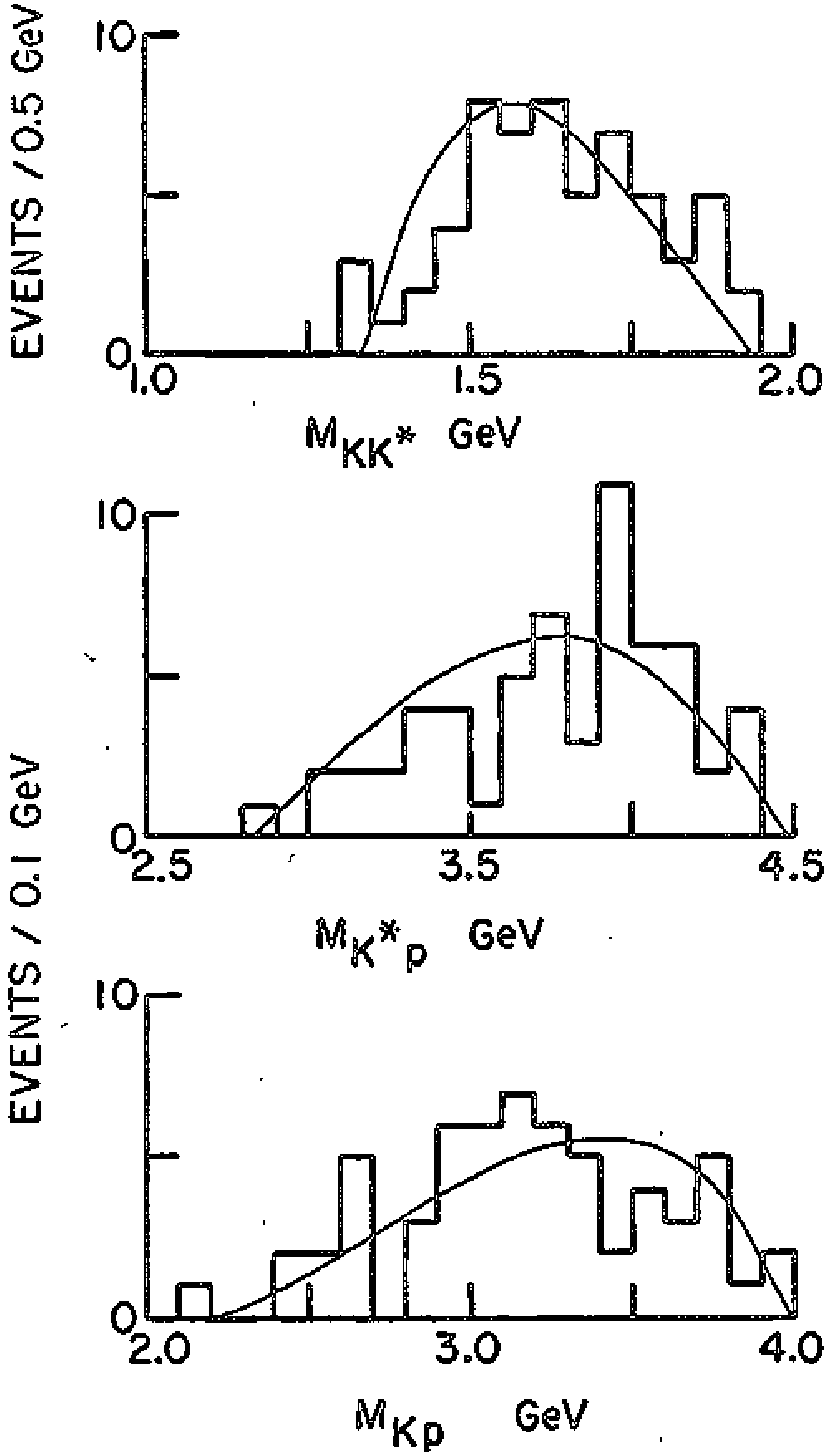

EVENTS / 0.5 GeV
10
0
1.0
1.5
2.0
$M_{KK^*}$ GeV
EVENTS / 0.1 GeV
10
0
2.5
3.5
4.5
$M_{K^*p}$ GeV
10
0
2.0
3.0
4.0
$M_{Kp}$ GeV

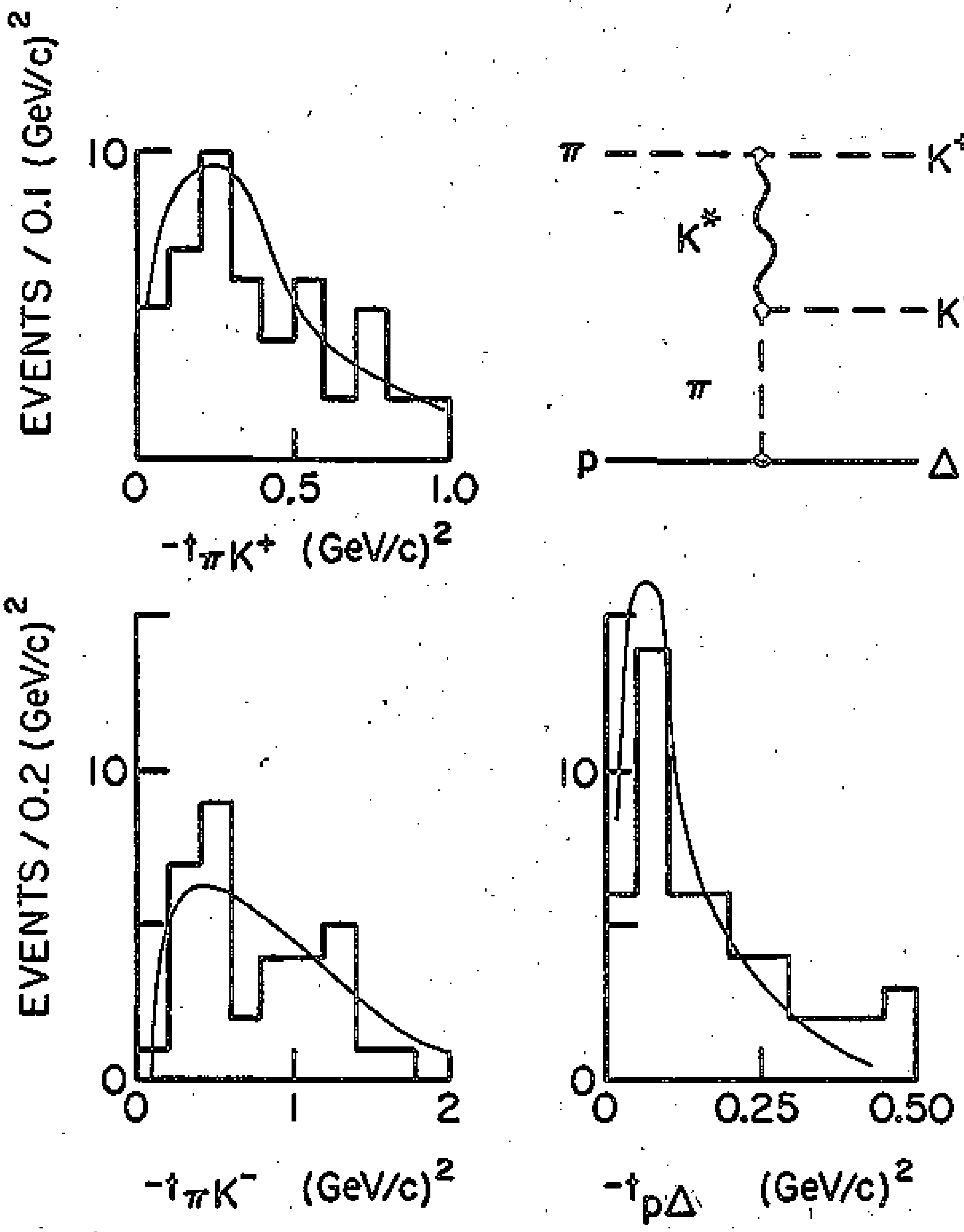

EVENTS / 0.1 (GeV/c)$^2$
10
0
0.5
1.0
$-t_{\pi K^+}$ (GeV/c)$^2$
π
K⁺
K*
K⁻
π
p
Δ
EVENTS / 0.2 (GeV/c)$^2$
10
0
1
2
$-t_{\pi K^-}$ (GeV/c)$^2$
10
0
0.25
0.50
$-t_{p\Delta}$ (GeV/c)$^2$

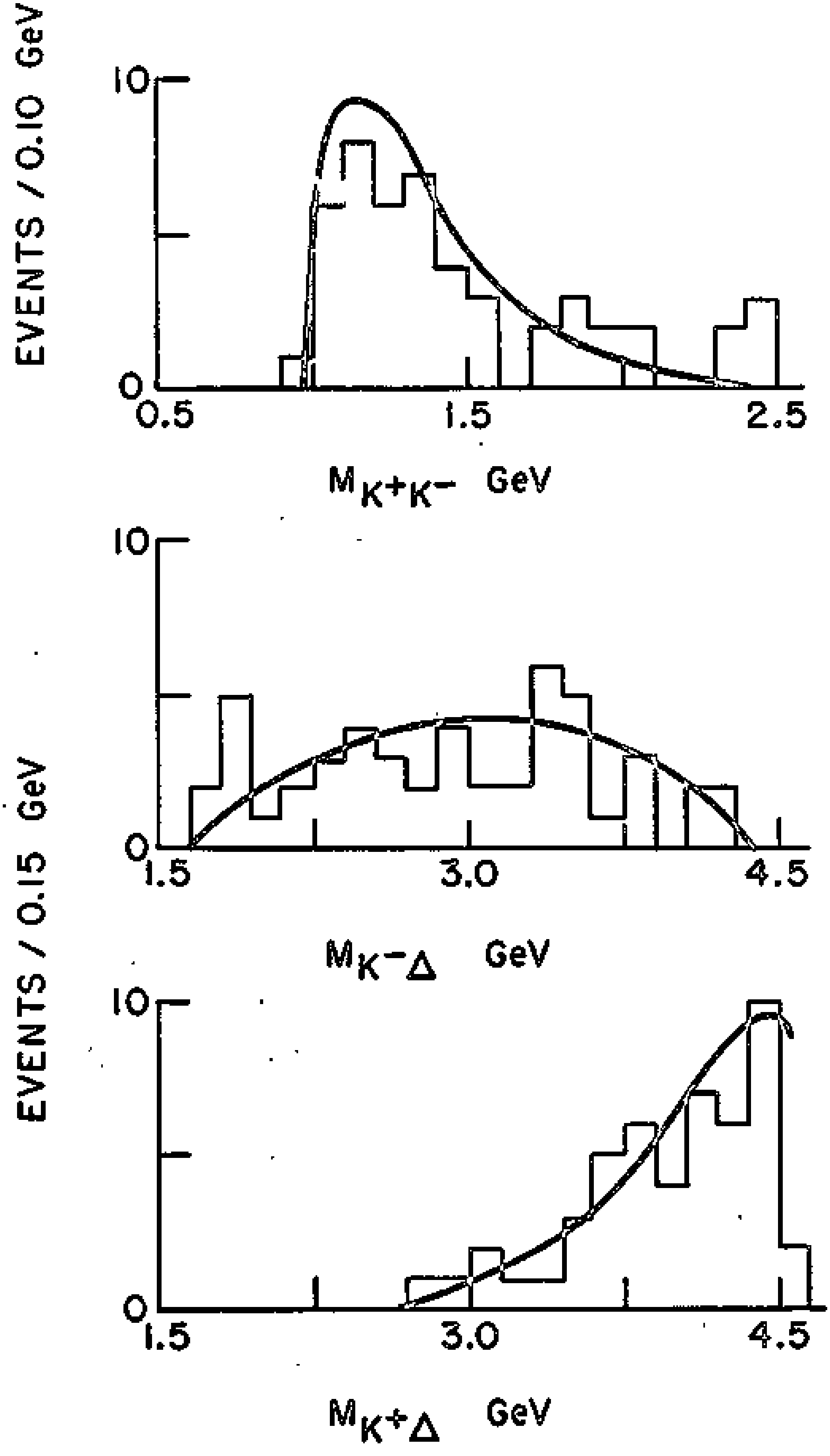
EVENTS / 0.10 GeV
10
0
0.5
1.5
2.5
$M_{K^+K^-}$ GeV
EVENTS / 0.15 GeV
10
0
1.5
3.0
4.5
$M_{K^-\Delta}$ GeV
10
0
1.5
3.0
4.5
$M_{K^+\Delta}$ GeV

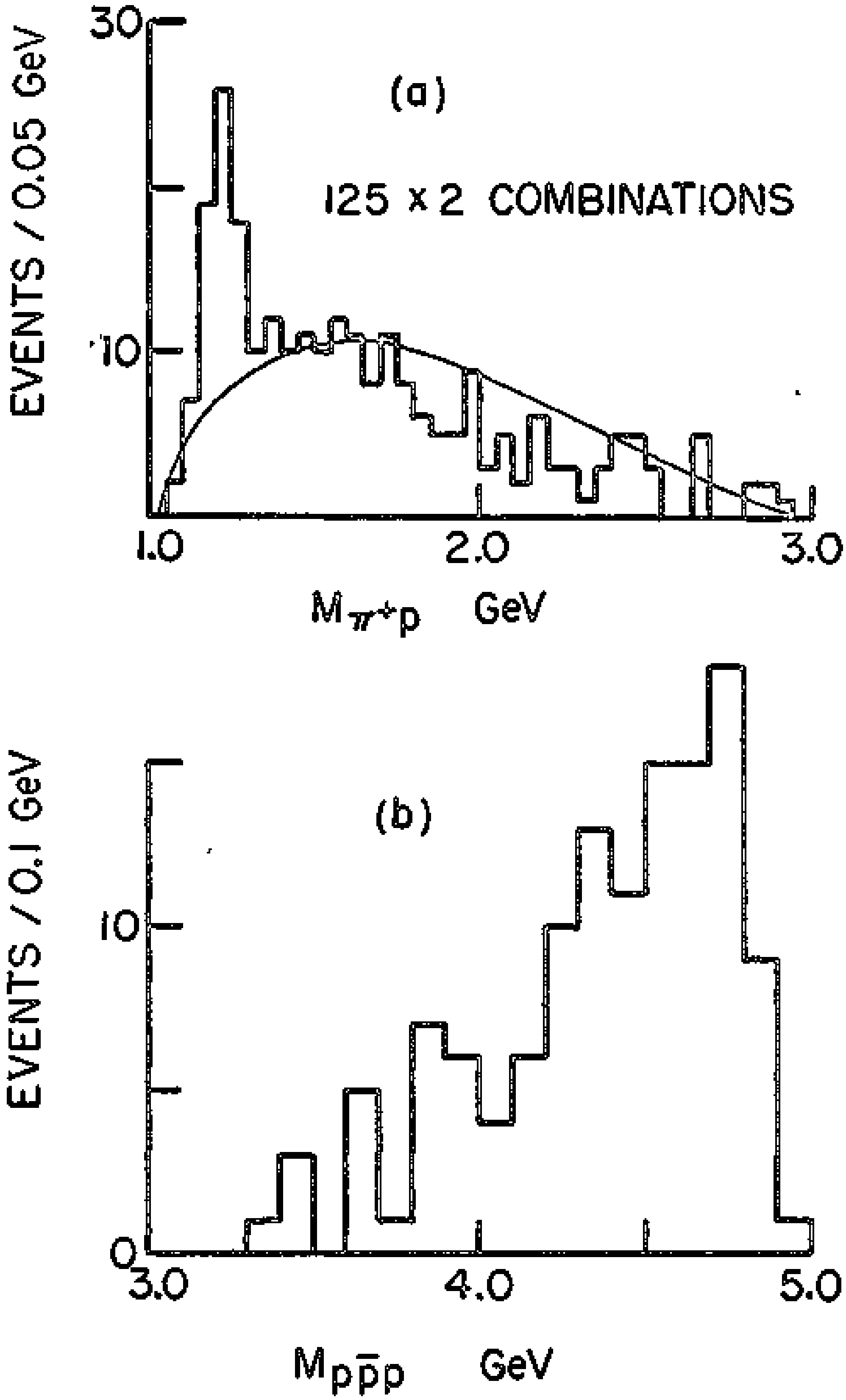

EVENTS / 0.05 GeV
30
10
(a)
125 x 2 COMBINATIONS
1.0
2.0
3.0
M π+p GeV
EVENTS / 0.1 GeV
10
0
(b)
3.0
4.0
5.0
M pp̄p GeV

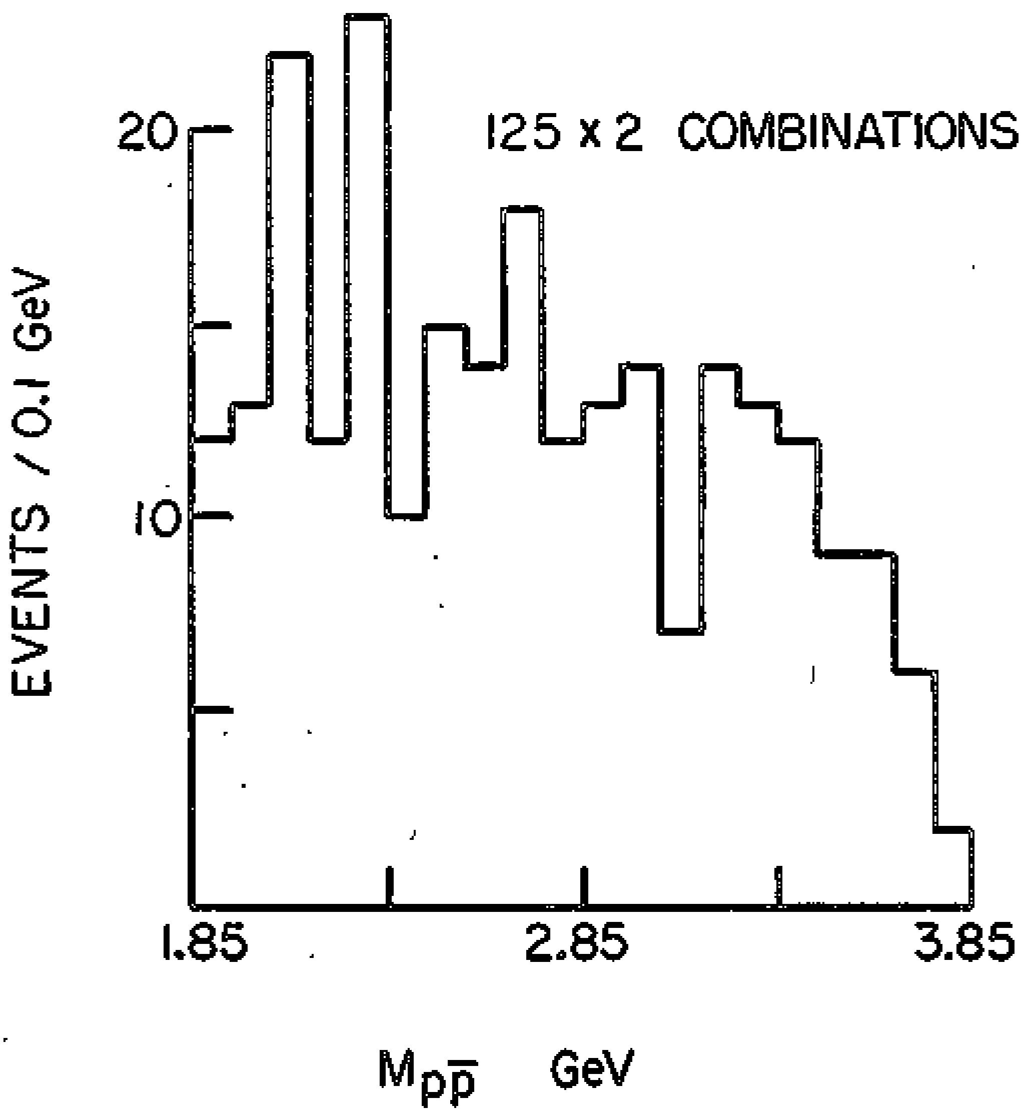
125 x 2 COMBINATIONS
EVENTS / 0.1 GeV
20
10
1.85
2.85
3.85
$M_{p\bar{p}}$ GeV